Understanding the effects of inhaler resistance on particle deposition behaviour – A computational modelling study

Computers in Biology and Medicine 167 (2023) 107673

Contents lists available at ScienceDirect

Computers in Biology and Medicine

journal homepage: www.elsevier.com/locate/compbiomed

Understanding the effects of inhaler resistance on particle deposition behaviour – A computational modelling study

Xinyu Cai [a], Jingliang Dong [b,c,*], Liam Milton-McGurk [d], Ann Lee [a], Zhiwei Shen [a], Hak-Kim Chan [e], Agisilaos Kourmatzis [d], Shaokoon Cheng [a]

[a] School of Engineering, Faculty of Science and Engineering, Macquarie University, Australia
[b] Institute for Sustainable Industries & Liveable Cities, Victoria University, PO Box 14428, Melbourne, VIC, 8001, Australia
[c] First Year College, Victoria University, Footscray Park Campus, Footscray, VIC, 3011, Australia
[d] School of Aerospace, Mechanical and Mechatronic Engineering, The University of Sydney, Australia
[e] Advanced Drug Delivery Group, Sydney Pharmacy School, Faculty of Medicine and Health, The University of Sydney, Sydney, New South Wales, Australia

ARTICLE INFO

Keywords:
Computational fluid dynamics
Dry powder inhalers
Inhaler resistance
Particle deposition

ABSTRACT

Background and objective: Understanding the impact of inhaler resistance on particle transport and deposition in the human upper airway is essential for optimizing inhaler designs, thereby contributing to the enhancement of the therapeutic efficacy of inhaled drug delivery. This study demonstrates the potential effects of inhaler resistance on particle deposition characteristics in an anatomically realistic human oropharynx and the United States Pharmacopeia (USP) throat using computational fluid dynamics (CFD).

Method: Magnetic resonance (MR) imaging was performed on a healthy volunteer biting on a small mockup inhaler mouthpiece. Three-dimensional geometry of the oropharynx and mouthpiece were reconstructed from the MR images. CFD simulations coupled with discrete phase modelling were conducted. Inhaled polydisperse particles under two different transient flow profiles with peak inspiratory flow rates (PIFR) of 30 L/min and 60 L/min were investigated. The effect of inhaler mouthpiece resistance was modelled as a porous medium by varying the initial resistance (Ri) and viscous resistance (Rv). Three resistance values, 0.02 $kPa^{0.5}minL^{-1}$, 0.035 $kPa^{0.5}minL^{-1}$ and 0.05 $kPa^{0.5}$ $minL^{-1}$, were simulated. The inhaler outlet velocity was set to be consistent across all models for both flow rate conditions to enable a meaningful comparison of models with different inhaler resistances.

Result: The results from this study demonstrate that investigating the effect of inhaler resistance by solely relying on the USP throat model may yield misleading results. For the geometrically realistic oropharyngeal model, both the pressure and kinetic energy profiles at the mid-sagittal plane of the airway change dramatically when connected to a higher-resistance inhaler. In addition, the geometrically realistic oropharyngeal model appears to have a resistance threshold. When this threshold is surpassed, significant changes in flow dynamics become evident, which is not observed in the USP throat model. Furthermore, this study also reveals that the impact of inhaler resistance in a geometrically realistic throat model extends beyond the oral cavity and affects particle deposition downstream of the oral cavity, including the oropharynx region.

Conclusion: Results from this study suggest that key mechanisms underpinning the working principles of inhaler resistance are intricately connected to their complex interaction with the pharynx geometry, which affects the local pressure, local variation in velocity and kinetic energy profile in the airway.

1. Introduction

Inhaled drug delivery is widely known as an effective approach to managing respiratory diseases. There are currently over 40 different dry powder inhalers in the market, and the industry is stipulated to reach $33 billion by 2023 [1]. Given the rising occurrence of Chronic Obstructive Pulmonary Disease (COPD) and asthma [2,3], developing new inhaler technologies through a deeper understanding of dominant factors contributing to efficacy is warranted. The intricate mechanisms governing the transport and deposition of dry powder drugs in the

* Corresponding author. Institute for Sustainable Industries & Liveable Cities, Victoria University, PO Box 14428, Melbourne, VIC, 8001, Australia.
E-mail address: jingliang.dong@vu.edu.au (J. Dong).

https://doi.org/10.1016/j.compbiomed.2023.107673
Received 26 June 2023; Received in revised form 29 October 2023; Accepted 6 November 2023
Available online 10 November 2023

airways following their release from inhalers are multifaceted and complex. This mechanism is influenced by various factors, including the inhaler mechanical design, the physical properties of the drugs, differences in airway geometries and inhalation flow profile [4]. Ideally, drugs should be deposited in the lower airways to achieve maximum effectiveness while minimizing medication deposition in the upper airway to reduce wastage and potential side effects.

Dry powder inhalers are designed to effectively deagglomerate and disperse drug formulations [5]. The variations in mechanical designs among inhalers can differ and may introduce flow-limiting effects associated with their resistance. Although the effects of inhaler resistance, such as how they affect dry powder transport and their deposition in the extrathoracic airway, have been studied, knowledge in this area remains fragmentary because the majority of existing work has compared inhalers with different designs, mouthpiece sizes and flow rate associated with the devices [6–13]. To gain a systematic understanding of the effects of inhaler resistance and the key mechanisms influencing their delivery effectiveness, controlling the mouthpiece sizes and flow rates would be beneficial. A widely acknowledged paradigm is that dry powder inhalers with high resistance are associated with a lower flow rate, which reduces the propensity of particle impaction and hence causes less deposition in extrathoracic airways. Conversely, a dry powder inhaler with low resistance tends to be associated with a higher flow rate, which may cause more particle deposition loss in the human pharynx. Clark et al. contended that, ultimately, the efficacy of a device prescribed to a population would depend on the mouth-inspiratory pressure an individual can generate while using the inhaler [14]. Indeed, inhaler resistance is an interesting and ongoing debate because the literature has reported somewhat conflicting data, which is challenging to resolve due to disparities in experimental conditions employed across various studies.

As a case in point, Yang et al. [12] showed that the extrathoracic deposition associated with the low resistance Osmohaler (0.021 $kPa^{0.5}minL^{-1}$) was ~80 %, and it is ~4 % less than the high resistance Osmohaler (0.036 $kPa^{0.5}minL^{-1}$). The study was performed at a flow rate of 65 L/min using the Alberta Idealized Throat (AIT). Below et al. [6] studied particle deposition in a pseudo-realistic paediatric mouth-throat model using the Novolizer (0.026 $kPa^{0.5}minL^{-1}$) and an inhalation flow profile with a peak flow rate of 51 L/min. In that study, particle deposition in the upper airway is 65 %. Given the similarity in inhaler resistance and inhaler mouthpiece sizes between the Novolizer (0.026 $kPa^{0.5}minL^{-1}$) and the low resistance Osmohaler (0.021 $kPa^{0.5}minL^{-1}$), it begs the question whether flow rate is the main factor that has constituted the discrepancies in deposition and the trend observed between the two studies (e.g. Yang et al. [12] and Below et al. [6]). The literature consists of many similar examples, where parameters used to conduct the experiments vary across studies. In the above comparison, differences in airway geometry and different inhalation flow profiles could also account for differences in the outcomes. Understanding what role inhaler resistance can play for a fixed flow rate exiting the inhaler and how it may affect the local velocity variations and subsequent pressure and kinetic energy profiles are essential to understand their impact on particle transport behaviour.

This research aims to shed light on how different inhaler resistances may potentially affect particle deposition in the pharynx using a numerical approach that couples computational fluid dynamics (CFD) with discrete phase modelling (DPM). The LRN k–ω SST model will be used for all models, given its demonstrated capabilities in predicting particle flow and deposition behaviour in existing research [15]. Three different inhaler resistances are modelled: 0.02 $kPa^{0.5}minL^{-1}$ (Breezhaler), 0.035 $kPa^{0.5}minL^{-1}$ (Turbuhaler) and 0.05 $kPa^{0.5}minL^{-1}$ (Handihaler), representing a range of low, mid and high inhaler resistances in the market [14,16–20]. To enable a meaningful comparison between devices, the average velocity at the outlet of the inhaler mouthpiece is controlled and kept the same, and resistance across the devices is modelled by prescribing porosity functions. We hypothesized that one of the predominant effects of inhaler resistance lies in the difference in pressure drop it can create, which can subsequently influence the pressure in the oral cavity and the local variation in velocity, leading to changes in kinetic energy. We will also test the concept that pharynx geometry plays an important role in determining the impact of inhaler resistance, and understanding this can be relevant to future inhaler device testing and development.

2. Method

A visual representation of the method is shown in Fig. 1.

2.1. Ethics attestations

The study was approved by the Human Research Ethics Committee of Macquarie University and conducted according to the Declaration of Helsinki. Informed written consent was obtained from the volunteer.

2.2. MR imaging

A 56-year-old subject (BMI: 39.5 kg/m^2) with no prior history of sleep or respiratory issues volunteered for this study. During the MR imaging, the subject was instructed to lie supine while biting on a mock-up inhaler with a mouthpiece size that matches the Breezhaler. Before the scan, the subject was trained to use and breathe through the inhaler without any aerosol present, and this was performed based on the inhaler instruction manual. Head pads were placed on the volunteers to prevent head movement during scanning. The participant held on to a buzzer, and notification was given before the scan commenced. The anatomical images were acquired using the following parameters. Field of view: 256 × 256, a 256 × 256 matrix size (1 mm × 1 mm pixel size), 6.8 ms repetition time, 3 ms echo time, 144 × 108 scan resolution, and 1 mm slice thickness. The scan duration lasted 6 min.

2.3. Model reconstruction

A 3D USP model and a geometrically realistic upper airway model (reconstructed from the MR images) were produced for this study. The geometrically realistic upper airway model was reconstructed from the MRI scans using 3D Slicer (www.slicer.org). During reconstruction, the airway boundaries were carefully defined using a threshold value to conserve most of the anatomical details of the upper airway. The model was subsequently exported as an STL file and converted to NURBS in Rhinoceros (Rhino 7, Robert McNeel & Associates, Seattle, Washington). A cylindrical inhaler extension, with a geometry representing the outlet of the Breezhaler, was also connected to the oral inlet of both the USP and the geometrically realistic upper airway model using Rhinoceros, and the latter was achieved by ensuring that the position of the inhaler is consistent with the MRI images.

Both models were imported into ANSYS ICEM-CFD (ANSYS Inc., Canonsburg, Pennsylvania) first to generate the tetrahedral/mixed unstructured meshes before converting them to polyhedral in Fluent. The geometrically realistic upper airway model was divided into seven sections: the inlet, inhaler, outlet, and four other regions that generally define the primary locations of the human pharynx, such as the oral cavity, oropharynx, laryngopharynx, and the trachea (Fig. 2). As this study aims to investigate the effects of 3 different inhaler resistance, a total of 6 models comprising 3 USP throats, and 3 geometrically realistic airways were generated.

2.4. Computational simulation

Discrete phase modelling (DPM) was used, and mannitol was chosen as the particle for the simulation. The density of the mannitol particles was defined as 1514 kg/m^3. The boundary condition at the inlet and outlet was prescribed as escape, while the walls of the inhaler and the

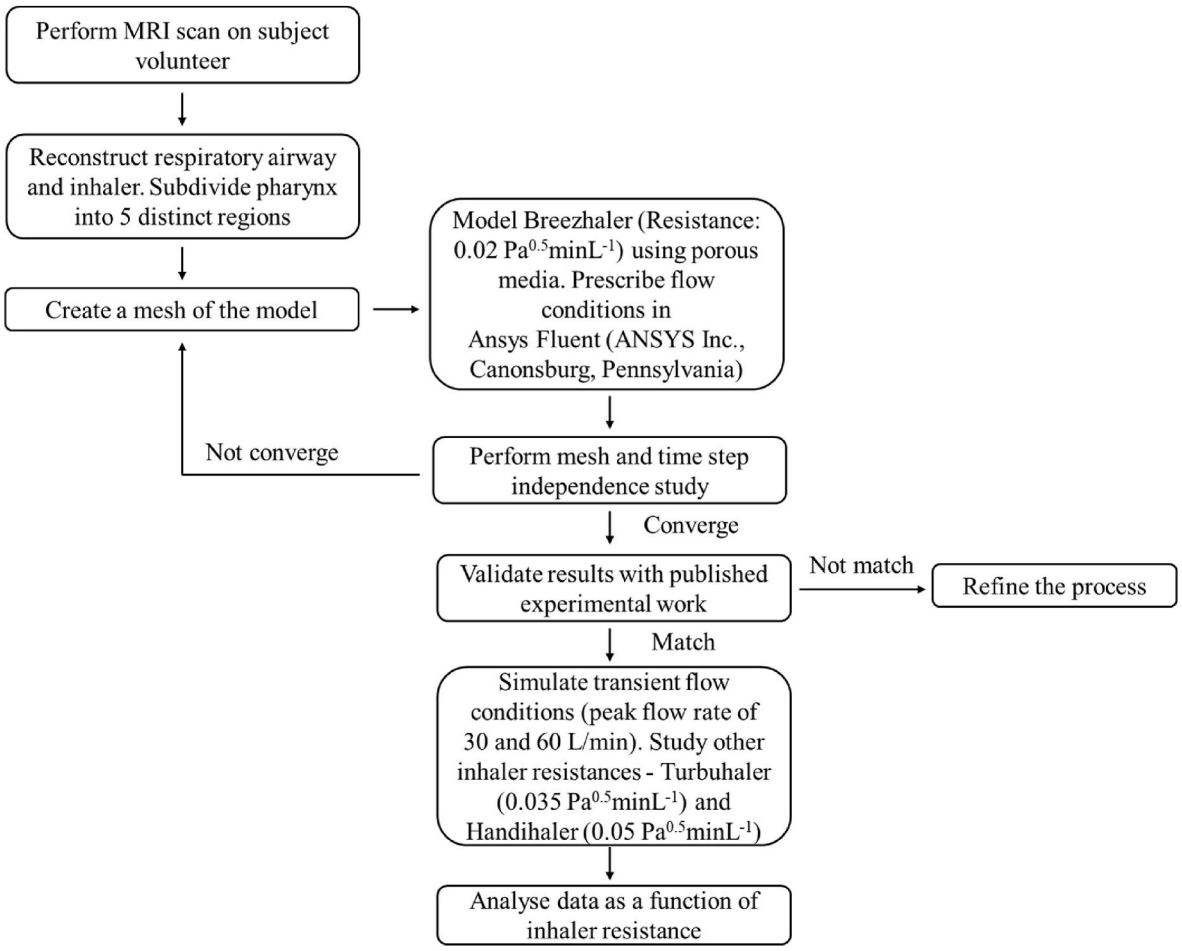

Fig. 1. Schematic of the working model.

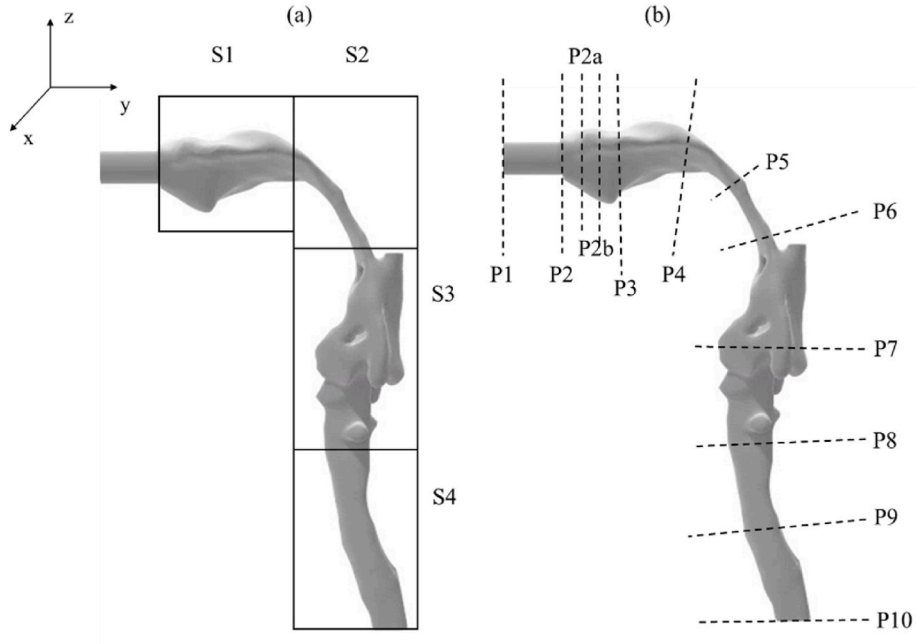

Fig. 2. Realistic upper airway. Panel A shows the airway is dissected into 4 primary regions where particle deposition is analyzed (S1- oral cavity, S2 - a segment of the airway connecting the oropharynx and the oral cavity, S3 - oropharynx, and S4 - trachea). Panel B shows 12 planes defined along the airway to analyze the average velocity, pressure and kinetic energy and how these change during inhalation.

entire pharynx were prescribed as trap. The porous zone was selected in the cell zone condition that represents the inhaler domain, and the porosity is defined by the viscous resistance (Rv), the inertial resistance (Ri) and the void ratio. These values are empirical, and Table 1 shows the pressure drop associated with the resistance of 0.02 $kPa^{0.5}minL^{-1}$, 0.035 $kPa^{0.5}minL^{-1}$ and 0.05 $kPa^{0.5}minL^{-1}$.

The turbulent intensity at the inlet was defined as 5 %, which has been commonly used in existing work on RANS simulations to represent fluid motion irregularities [21–23]. The viscosity ratio for the inlet was prescribed as 10 %. A few preliminary case studies were performed before the actual studies in order to test different boundary conditions and they were: 1) generating flow across the inhaler-pharynx system by prescribing velocity at the inhaler inlet, 2) generating flow across the inhaler-pharynx system by prescribing a pressure difference across the model (prescribing non-zero pressure at the pharynx outlet), and 3) using other combinations of Rv, Ri and porosity to produce the same resistance intended for this study to understand their effects on flow in the porous domain. Results from this preliminary work showed no considerable differences in the flow field between the cases. Thus, the velocity inlet boundary condition was applied at the inlet for all models (See Fig. 3). The SIMPLE algorithm and convergence criterion of 10^{-5} was used for pressure-velocity coupling. The model was imported into ANSYS FLUENT (ANSYS Inc., Canonsburg, Pennsylvania) for simulations, using double precision and parallel processing with six processors. A realistic inhalation flow profile, extracted from a previous work published by the authors [24] was used. All simulations started with a steady-state analysis, and the results were used as initialization conditions for the transient simulations with an overall time duration of 4 s time, with a time step size of 0.01s. Mesh independence test, injected particle number independence test and time step size independence test were all done in our previous paper [25].

2.5. Governing equations

The porous media model functions as a momentum sink in the governing momentum equation [26] and is represented in the equation by a momentum source term, which consists of two parts: a viscous loss term (Darcy, the first term in Equation (1)) and an inertial loss term (the second term in Equation (1)).

$$S_i = -\left(\sum_{j=1}^{3} D_{ij}\mu v_j + \int_{j=1}^{3} C_{ij}\frac{1}{2}\rho|v|v_j\right) \quad (1)$$

where Si is the source term for the ith momentum equation for x, y, and z direction, D and C are prescribed matrices, |v| is the velocity magnitude, and v_j is the velocity vector in y direction. This momentum sinks decrease pressure proportional to the fluid velocity or the square of the velocity within the cell. Equation (1) can then be simplified to Equation (2) to model the scenario of a simple homogeneous porous media.

$$S_i = -\left(\frac{\mu}{\alpha}v_i + C_2\frac{1}{2}\rho|v|v_i\right) \quad (2)$$

here α is the permeability, and C_2 is the inertial resistance factor. Equation (2) is derived by assigning the "D" and "C" in Equation (1) as diagonal matrices by having 1/α and C_2 on their diagonals, respectively, with all other elements as zero.

When the flow velocity is high, the constant "C_2" in Equation (1) compensates for the inertial losses in the porous medium. This constant can be considered as a coefficient of loss per unit length in the flow direction, making it possible to express the pressure drop as a function of the dynamic head. In this study, the term permeability was not used as it is not relevant to the simulation in the present study, only inertial loss is considered, resulting in the form of the porous media equation shown in Equation (3).

$$\nabla p = -\sum_{j=1}^{3} C_{2ij}\left(\frac{1}{2}\rho v_j|v|\right) \quad (3)$$

which can be written in terms of the pressure drop in the x, y, z directions as:

$$\Delta p_x \approx \sum_{j=1}^{3} C_{2xj}\Delta n_x\frac{1}{2}\rho v_j|v| \quad (4)$$

$$\Delta p_y \approx \sum_{j=1}^{3} C_{2yj}\Delta n_y\frac{1}{2}\rho v_j|v| \quad (5)$$

$$\Delta p_z \approx \sum_{j=1}^{3} C_{2zj}\Delta n_z\frac{1}{2}\rho v_j|v| \quad (6)$$

where Δn_x, Δn_y, or Δn_z represents the thickness of the medium in x, y, and z directions, respectively.

The particle sizes in the simulations were modelled based on the size distribution of mannitol depicted in Fig. 4. This was achieved using a DPM model and a user-defined file with 8000 particles randomly distributed at the inhaler inlet. The equation that governs the three-dimensional particle transport behaviour was derived from Equation

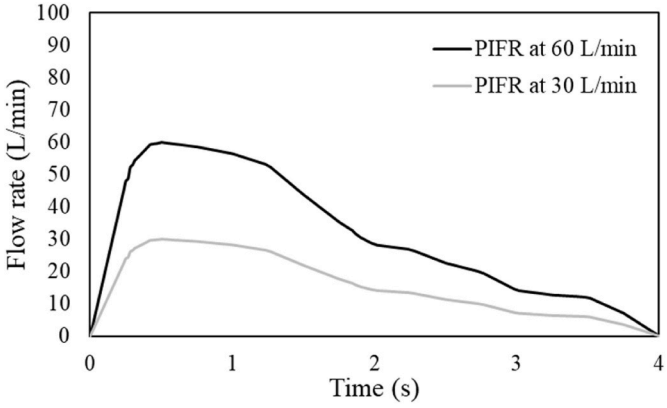

Fig. 3. Inspiratory inhalation profile.

Table 1
Inhaler resistance and pressure drop parameters.

Case	Inhaler Resistance (kPa^ (1/2) L/min)	Pressure drops at 30 L/min (Pa)	Pressure drops at 60 L/min (Pa)
1	0.02	360	1440
2	0.035	1102.5	4410
3	0.05	2250	9000

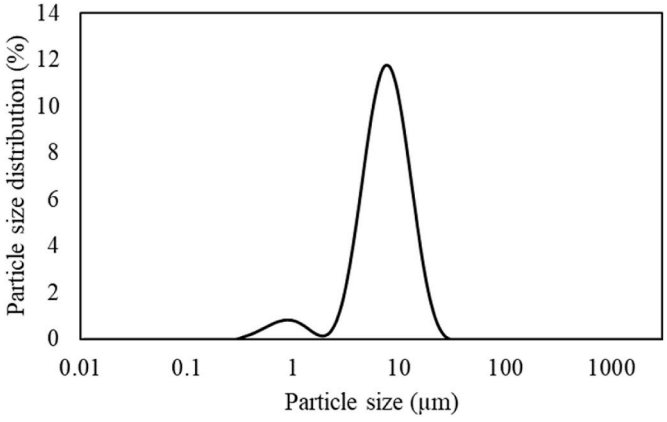

Fig. 4. Particle size distribution.

(7) [26].

$$\rho_p dp \frac{d^2 xp}{dt^2} = \frac{3}{4}\rho C_D(v - vp)|v - vp| + \rho_p dpg \quad (7)$$

Where g is the gravity vector (9.81 N/kg) with a -x direction, ρ is the flow density, ρ_P is the particle density, x_P is the particle displacement, d_P is the particle diameter, C_D is the drag force coefficient, v is the flow velocity (m/s), and v_p is the particle velocity (m/s).

Since the simulation involved particles with varying sizes, Equation (8) was utilized to evaluate the deposition efficiency (DE).

$$DE\% = \frac{Mass\ of\ deposited\ particles}{Mass\ of\ injected\ particles} * 100\% \quad (8)$$

3. Results

3.1. Validation of computational models with published experimental studies

The deposition efficiency of mannitol particles in the USP throat models with a low resistance (0.021 $kPa^{0.5}minL^{-1}$) prescribed to the inhaler at steady state flow of 40 L/min, 60 L/min and 80 L/min is shown in Fig. 5. Results from those models match well with the experimental data reported by Cheng et al. [27], which were conducted with the same flow conditions and particle size band. The percentage variations between the computational models and the experimental result for flow rates of 40 L/min, 60 L/min and 80 L/min are 1.8 %, 2.68 %, and 2.62 %, respectively. In Cheng et al. [27], high-performance liquid chromatography was used to measure the particle mass to determine the particle deposition in the upper airway. Both data sets show that deposition in the USP throat increases gradually with higher flow rates under steady-state flow conditions, confirming that the model can capture the experiment's overall physical behaviour.

3.2. Effects of inhaler resistance on particle deposition characteristics in the upper airway

Fig. 6 summarizes the total particles deposited in the USP and realistic upper airway models with three different inhalers. The models are simulated using a transient inhalation flow profile described in Fig. 3. While there appears to be a general upward trend in particle deposition for both the USP throat and geometrically realistic upper airway cases, this trend is somewhat plateaued for the USP cases, demonstrating that the effect of inhaler resistance is more pronounced in a realistic upper airway. A simplified pharynx replica such as the USP throat may not be able to recapitulate the distinctive effects associated with higher inhaler resistance when used in the geometrically realistic upper airway. The results further indicate that deposition in the USP throat and geometrically realistic airway are more similar for the mid and high-resistance cases but are considerably different for the low-resistance case. This may suggest the need to interpret experimental outcomes carefully when the USP induction port is used to study low-resistance inhalers experimentally. There are several plausible reasons why the USP computational model with low resistance has more deposition than the realistic airway model. For example, the transition in geometry between the small inhaler mouthpiece and the large USP inlet is abrupt, unlike the realistic airway model. Such abrupt change in geometry connectivity is likely to have increased recirculation at the USP throat inlet that promotes deposition, contrary to the realistic airway model, where the streamlines of the jet flow carry the particles through the airway. Based on the two peak flow rates (30 L/min and 60 L/min) chosen for this study, it also appears that deposition efficiency in the realistic airway is not strongly affected by the flow rate magnitude, especially for the low and mid-resistance cases. Note that this observation does not apply to a USP throat. For example, as shown in Fig. 4, the effect of flow rate on much simpler geometries is more apparent, and this is likely because simpler geometry is less capable of trapping particles at lower flow rates. In the realistic airway cases tested in Fig. 5, the effects of flow rate interestingly become more apparent for the high-resistance case, with the difference in deposition efficiency being ~10 % between the two flow rates for the geometrically realistic airway model.

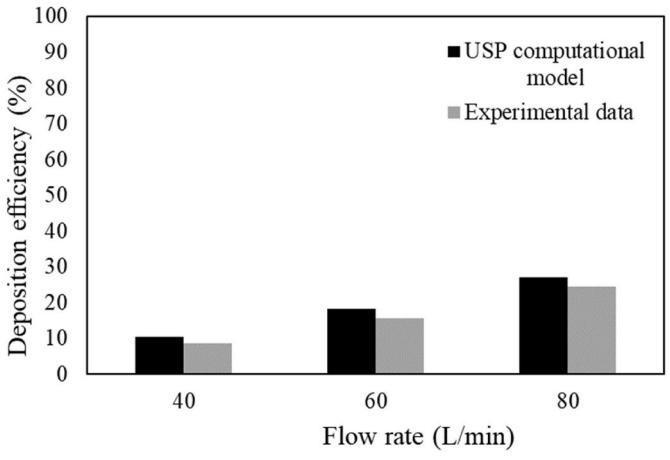

Fig. 5. Deposition efficiency of mannitol in the USP models at 40 L/min, 60 L/min and 80 L/min between simulation results and existing paper [27].

Fig. 7 (a) shows the regional particle deposition in the four different airway sections of the geometrically realistic upper airway model for all the 30 L/min peak flow rate cases. Regardless of the differences in inhaler resistance, deposition is concentrated in section 2 of the airway and has a similar mass quantity of particles deposited in sections 1 (the oral cavity) and 3 (the oropharyngeal region). In both these sections (sections 1 and 3), particle deposition is also less than 12 % for all the models. Inhaler resistance also appears to have a dramatic effect on particle deposition in section 2, such that there appears to be a non-linear and increasing trend of particle deposition with higher inhaler resistance. Potential reasons behind these and later observations to be presented in this section will be provided in the discussion section of this paper.

Fig. 7 (b) shows the regional particle deposition in the four different airway sections of the geometrically realistic upper airway model for all the 60 L/min peak flow rate cases. In the oral cavity (section 1), particle deposition is the highest for the high-resistance case and lowest for the low-resistance case. The difference in deposition between the low and high-resistance here is approximately four-fold, with the high-resistance inhaler reaching a deposited mass fraction of 61 %. In section 2, deposition is the highest for the mid-resistance inhaler but lowest for the low-resistance inhaler. All three inhalers have negligible deposition at the oropharynx (section 3) and larynx (section 4) regions, and this is likely because most of the particles have been trapped in the first two sections of the pharynx.

3.3. Airflow dynamics

3.3.1. USP model

Fig. 8 shows the velocity magnitude, pressure and turbulence kinetic energy contours at the mid-sagittal plane for the USP models at different time points of the inhalation cycle. Based on the results, it can be observed that close to the onset of inhalation (at T = 0.1s), both the velocity and pressure contour appear to be the most affected by inhaler resistance. It can be further observed that this effect extends beyond the horizontal section of the USP throat, and some differences in the velocity contour can be observed downstream of the simple airway replica (see circled insets). Inhaler resistance does not appear to affect the flow dynamics significantly at T = 0.3 s or T = 0.5 s. Overall, the results presented here indicate that despite large changes in inhaler resistance and having the average velocity controlled at the inhaler outlet, these

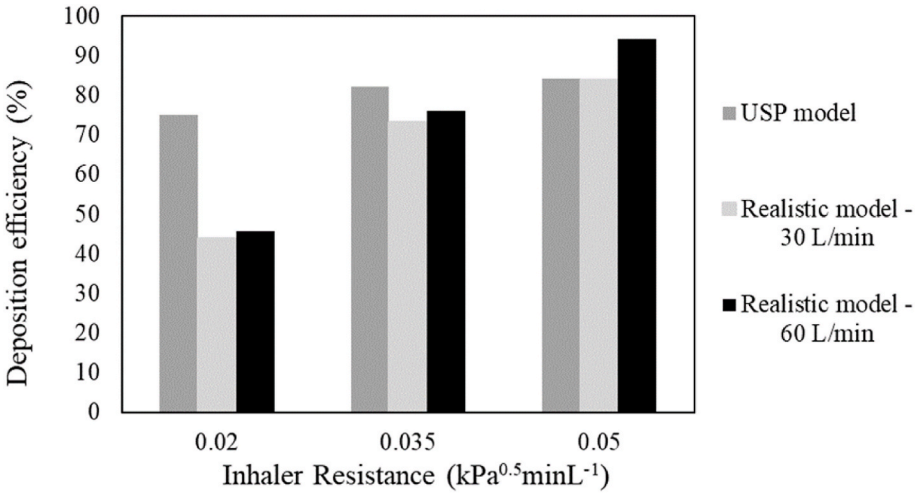

Fig. 6. Deposition efficiency of USP model and realistic upper airway models with three different resistances.

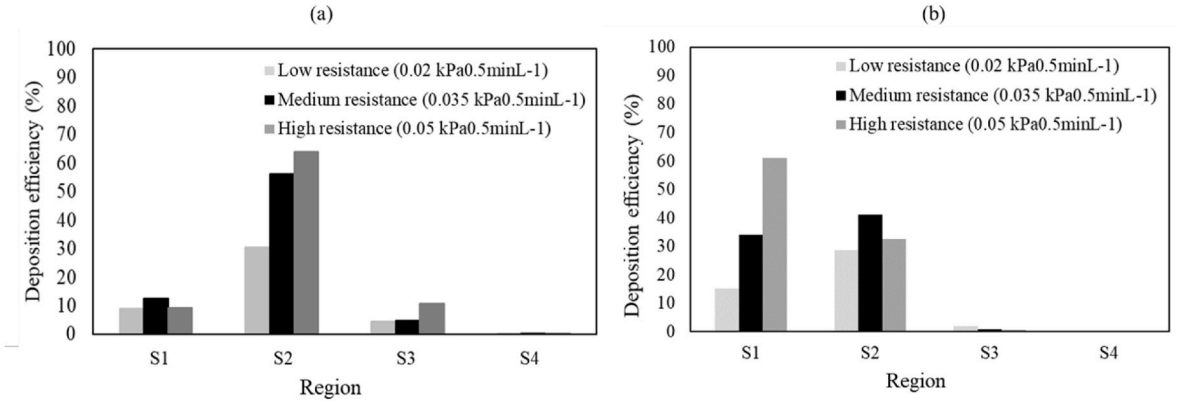

Fig. 7. Regional deposition efficiency in the realistic upper airway models with three different resistances where (a) is for 30 L/min and (b) is for 60 L/min.

effects do not seem to substantially influence the flow field computed in the USP throat, though some variations are noticeable. These results are consistent with the particle deposition data, where only small changes in particle deposition are observed in the USP throat for a change in resistance at a fixed flow rate despite the significant differences in inhaler resistance modelled.

3.3.2. *Geometrically realistic airway models*

Fig. 9 shows the velocity magnitude contours at the mid-sagittal plane of the geometrically realistic upper airway models at different times of the inhalation profile. Similar to the USP throat, flow dynamics appear to be the most affected by inhaler resistance close to the onset of inhalation. Specifically, it can be noted that the differences are apparent at the oropharynx region, adjacent and caudal to the epiglottis. The velocity ranges from 0 to 10.5 m/s at the oropharynx (see rectangle inset) across all models. Although this velocity magnitude is consistent between the models, there is a slight disparity in the velocity contour pattern. Notably, the model with the highest inhaler resistance showcases the highest average velocity within the inset, as observed on the midsagittal plane.

Fig. 10 shows the pressure contours. It is important to note that these pressure profiles do not represent realistic inspiratory mouth pressure as the models did not consider the entire respiratory airways. The results here, though, show how inhaler resistance could potentially affect the pressure change and its distribution within the airway, and specifically, how they differ at different periods of inhalation. In the oral cavity, a significant change in pressure within the oral cavity occurs between T = 0.1 to T = 0.3 s, but this is not observed in the model with the highest inhaler resistance. The change in average pressure (between T = 0.1 and 0.3 s) in the oral cavity are 552 Pa and 495 Pa for the low and mid-resistance inhaler models, respectively. Another observation is that, at the onset of inhalation, (T = 0.1s), pressure in the oral cavity does not appear to be significantly different between the low and mid-resistance inhaler cases but is different between the mid and high-resistance cases. The above may suggest a threshold effect for inhaler resistance such that when exceeded, it could change the local conditions of the airway, which can subsequently influence particle transport in a way that is different to a similar inhaler design but of lower resistance. This merits further investigation. Similar to previous computational modelling work that has investigated pressure dynamics in sleep apnoea [28], the pharynx section that demonstrates the most significant change in pressure is close to the tip of the soft palate, at the velopharynx, which is one of the narrowest regions of the upper airway. The above information discussed in the context of pressure dynamics is consistent with observations of the turbulence kinetic energy (TKE) described in the following section.

As shown in Fig. 11, at T = 0.1 s, the TKE contour in the oral cavity is somewhat similar between the low and mid inhaler resistance cases, but they are different from the high inhaler resistance case. For the high inhaler resistance case, high TKE can be observed in section 2 of the airway. The TKE is also comparatively higher for this case throughout the inhalation (e.g., at all the time points investigated). Here, the concept of a threshold effect in terms of the inhaler resistance appears to be at play, such that when the resistance is exceeded, it results in a

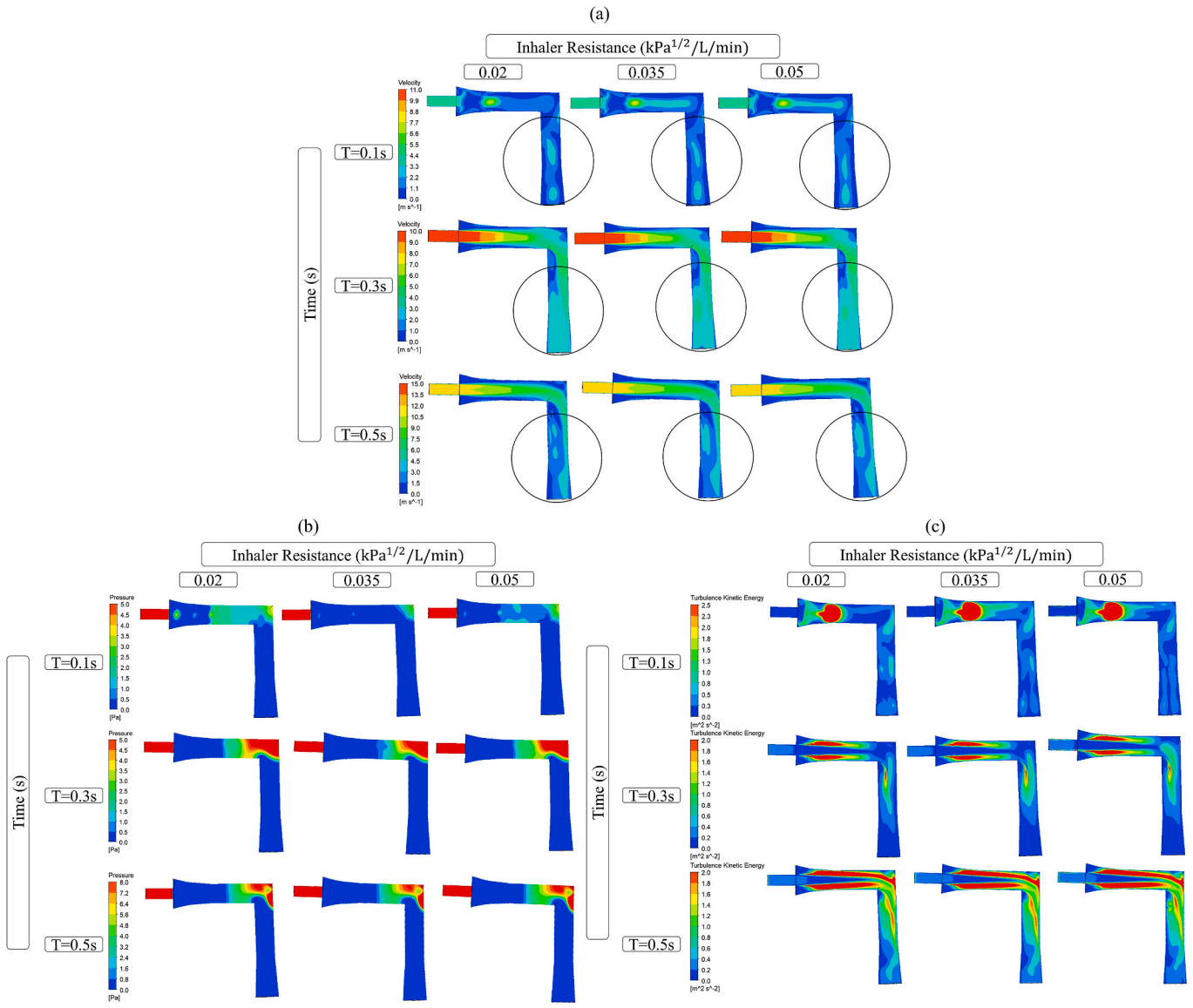

Fig. 8. Contours for the USP model with three different resistances at three time points at 60 L/min, where (a) for velocity contours, (b) for pressure contours, and (c) for kinetic energy contours.

significant change in flow dynamics (and TKE) that may lead to high oral deposition, as seen in Fig. 7.

Fig. 12 shows the transient change in spatially averaged velocity magnitude, pressure and kinetic energy across 10 planes (see Methods; Fig. 2) situated at different locations along the upper airway. While all three models give similar trends for the average velocity, pressure and turbulence kinetic energy along the airway (and in time), the present results suggest that the influence of inhaler resistance is most significant close to the onset of inhalation, with differences among the cases diminishing over time.

The turbulence kinetic energy appears to be the most significantly affected by inhaler resistance. This can also be seen in Fig. 13, which shows the spatially averaged turbulence kinetic energy in sections 1-4, with the largest difference occurring in section 1 for 60 L/min. The results show that turbulent kinetic energy increases with resistance, with a substantial increase between the 0.035 and 0.05 kPa$^{0.5}$minL^{-1} cases. Fig. 7(b) shows that deposition in section 1 increases with resistance, which is alluring to attribute to the increase in turbulence kinetic energy. However, given that such observations are \not consistent across all the sections and flow rates, the above suggests that while turbulence plays a role in the local deposition mechanics, turbulent kinetic energy alone is likely insufficient to explain the differences in deposition arising from varying inhaler resistance.

4. Discussion

A key challenge in understanding inhaler efficacy and comparing commercial inhalers with varying resistance is the difficulty of controlling air velocity exiting the inhaler. Adding to the complexity is the variability in mouthpiece sizes, which changes oral cavity space and the inhaler's outlet, affecting the velocity. A common contention on the working principle of inhalers is that high-resistance inhalers limit flow, reducing velocity and affecting particle transport. Without controlling the inhaler outlet air velocity and the mouthpiece size, it is difficult to elucidate the true effects of inhaler resistance, which is associated with the drop in pressure across the devices in studies involving humans. Hence, despite the number of research published to compare efficacies between inhalers, it was generally challenging to meaningfully interpret the data. This study illustrates how the above predicament can be resolved and that insights into the working principles of inhaler

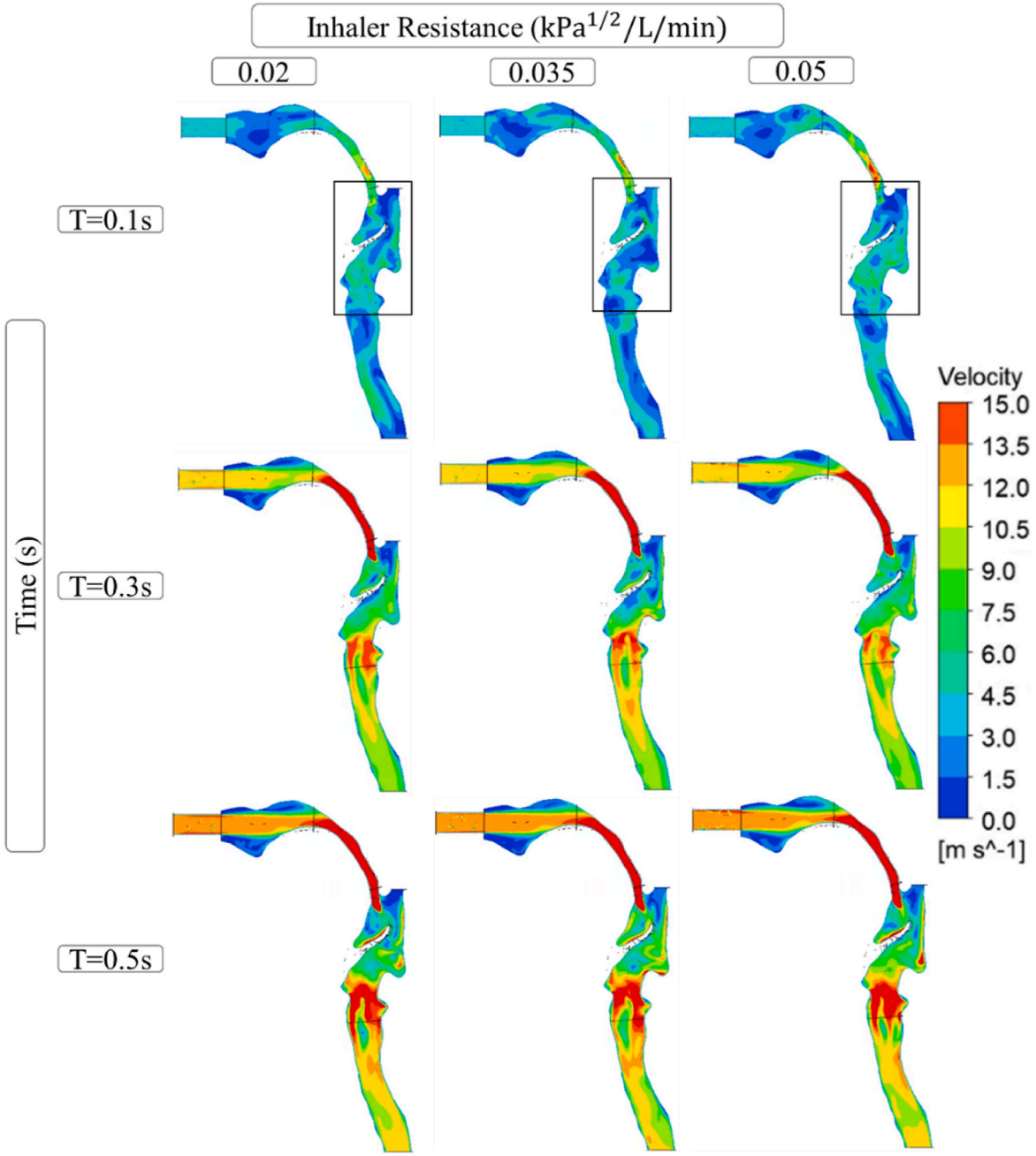

Fig. 9. Velocity contour of realistic upper airway models at 60 L/min.

resistance can be effectively unveiled through computational models. To the best of the authors' knowledge, this manuscript is the first to describe how inhaler resistance may be modelled by using porous media. By modelling the inhaler resistance as porous media, the work shows how velocity can be controlled at the outlet of an inhaler design. It demonstrates that despite having the same velocity, particle transport and deposition differ between the models with different inhaler resistance. The results suggest that the efficacy of an inhaler probably has little to do with the air velocity exiting the inhaler but with the kinetic energy and pressure drop developed across a given device. A caveat to note in this study concerns its application to practical inhaler systems, given that the inhaler resistance has been modelled by inducing drag forces across a porous medium, which is different to how most inhalers in the market have been designed. However, when interpreted carefully, the results from this current work suggest useful information that may be considered when analysing inhalers' efficacy and their design. First, investigating the effect of inhaler resistance using a USP throat may yield misleading results. This study demonstrated that when compared to a geometrically realistic airway model, the USP throat yields a lower particle deposition for inhalers with high resistance but a higher particle deposition for inhalers with low resistance. Second, the results suggest that interactions between inhaler resistance and a geometrically realistic human pharynx may exhibit a threshold effect. When the resistance level is exceeded, it is likely to alter the flow dynamics significantly. Given that the threshold effect is obvious in the geometrically realistic airway cases but not in the USP throat cases, this suggests that the resistance threshold may differ between humans, depending on the complexity and inherent resistance of the airways. Finally, implications of flow dynamics from using different inhaler resistances are not limited to the oral cavity, and appear to extend downstream, which led to variability in particle deposition at the oropharynx.

In this current work, the basic USP computational model (with a low

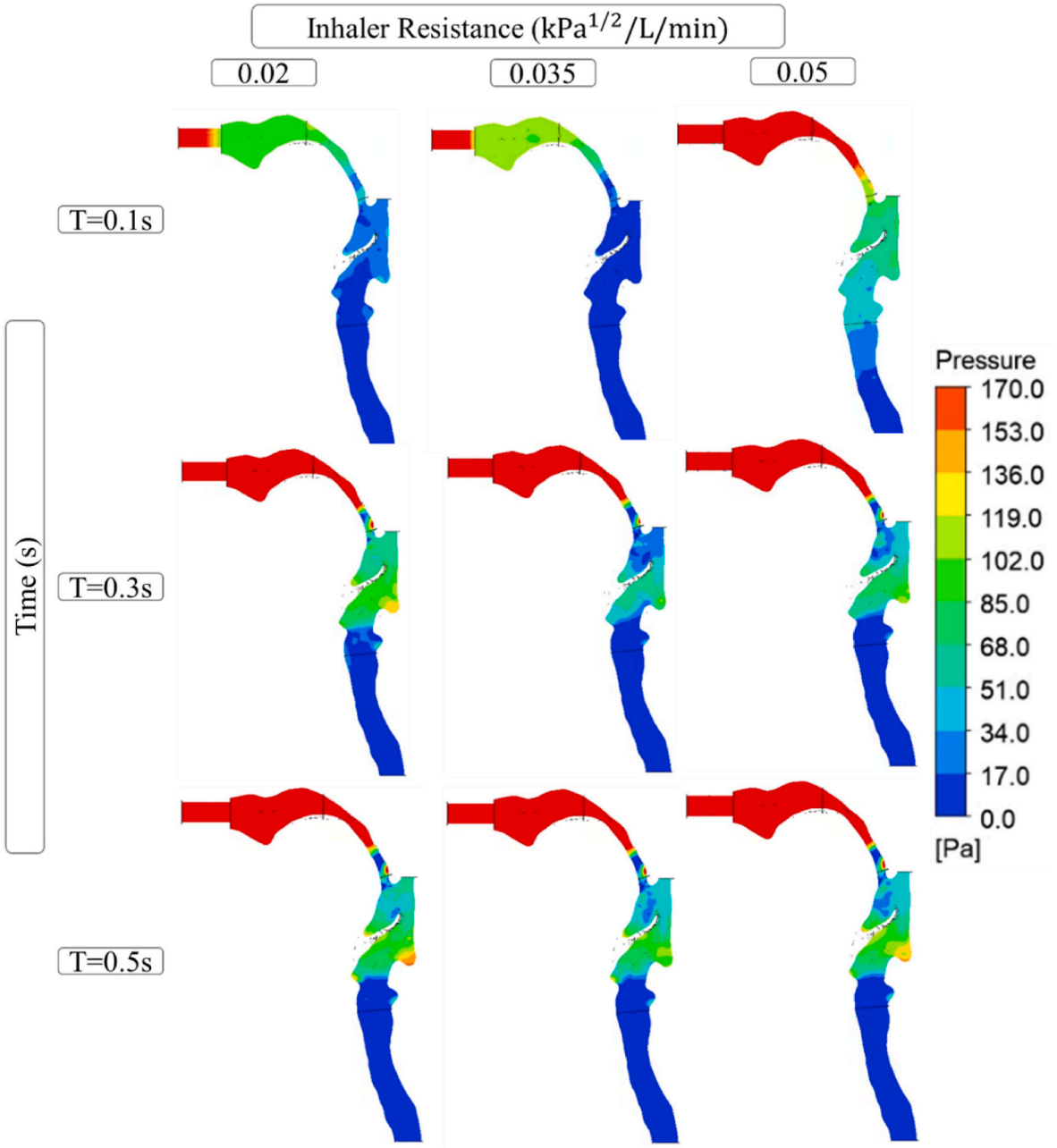

Fig. 10. Pressure contour of realistic upper airway models at 60 L/min.

inhaler resistance, 0.021 kPa$^{0.5}$minL^{-1}) was validated with the experimental data produced by Cheng et al. While there is a close correspondence between the results, which validated the accuracy of the computational model used in this current work, the following discussion extends this subject by comparing the results from this study with other work done in this area. Huang et al. [29] studied particle deposition in the USP throat using particles of different size bands and flow rates. The study by Huang et al. [29] showed that there was around 14 % deposition in the computational USP throat model when simulating monodisperse particles of 3 μm at flow rates of 60 L/min. The results are again very similar to those produced by the USP computational model in this current work, where a deposition of 18 % was observed. The following table summarizes some experimental studies and their measurements on particle deposition using inhalers with different resistance. These studies are included because the experimental conditions used to conduct the studies are close to the computational modelling conditions specified in this current work. The flow conditions, for example, have all been performed at close to 60 L/min, or having a peak flow rate of 60L/min, when transient flow has been used to conduct the studies.

Table 2 reveals that despite uniform resistance, flow rates, and realistic upper airway geometries in existing studies, deposition data can significantly differ. Lindert et al. [9] investigated the performance of dry powder inhalers with single-dose capsules in preschool children and adults using the AIT. The AIT encompasses essential anatomical attributes of the human upper airway. These attributes include the soft palate and epiglottis [22,30]. Consequently, the AIT is, hence, a fitting model to enable meaningful comparisons with the outcomes of the current study. In the work of Lindert et al. [9], particle deposition in the upper airway associated with the Handihaler is 65 %, which is approximately 30 % lower than the current study. However, the results of the Cyclohaler with a low resistance (in the same study of Lindert et al. [9]) yielded a deposition of 38 %, and this is comparable with our deposition result of 45 %. A point to note is that the experimental data produced by Lindert et al. [9] is based on steady-state flow, whereas the

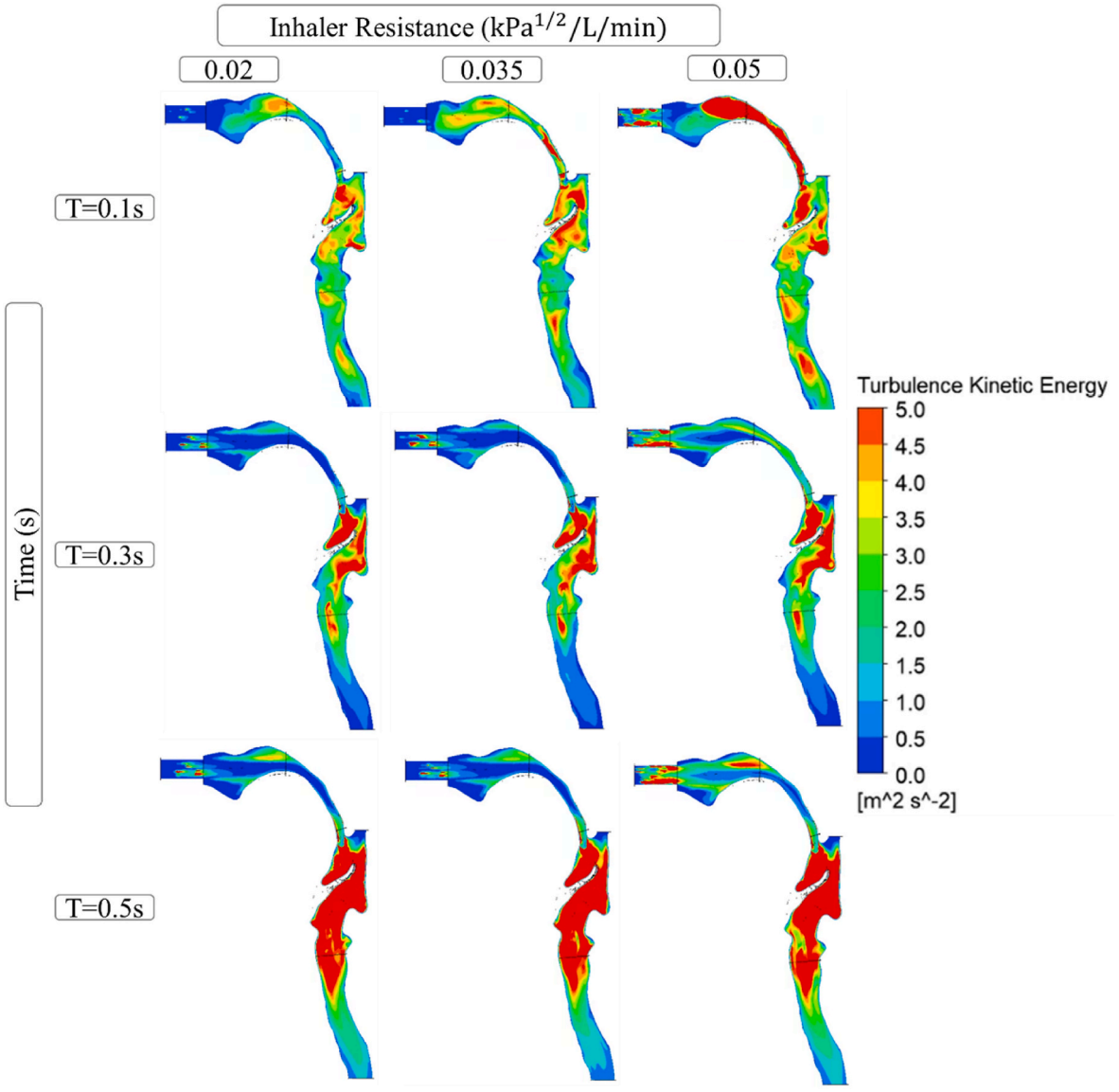

Fig. 11. Turbulent kinetic energy contour of realistic upper airway models at 60 L/min.

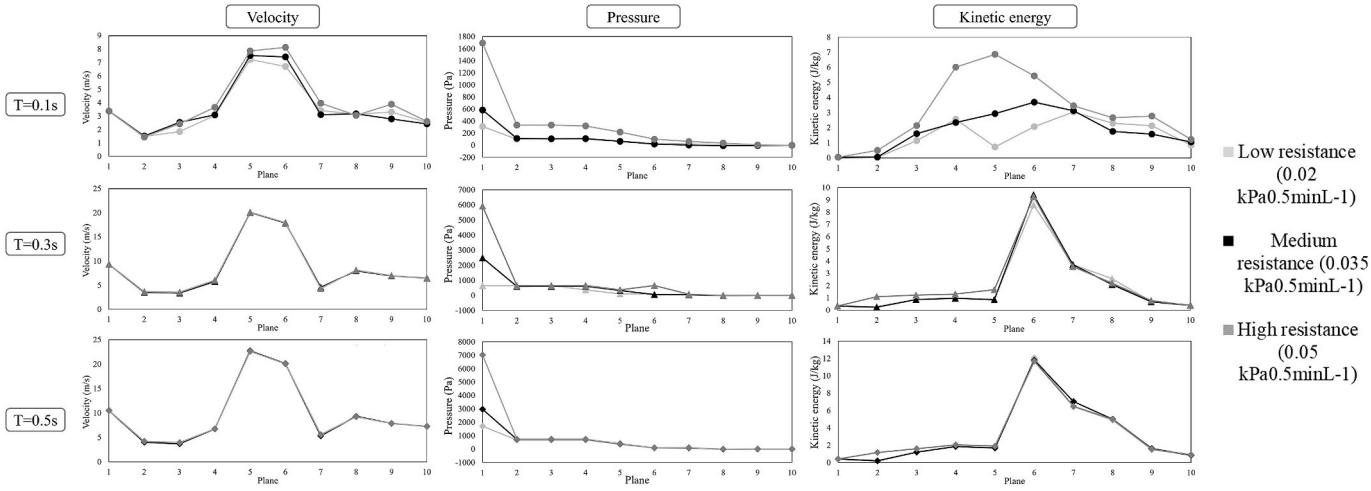

Fig. 12. Mean velocity, pressure, and kinetic energy at ten planes along the realistic upper airway models at 60 L/min.

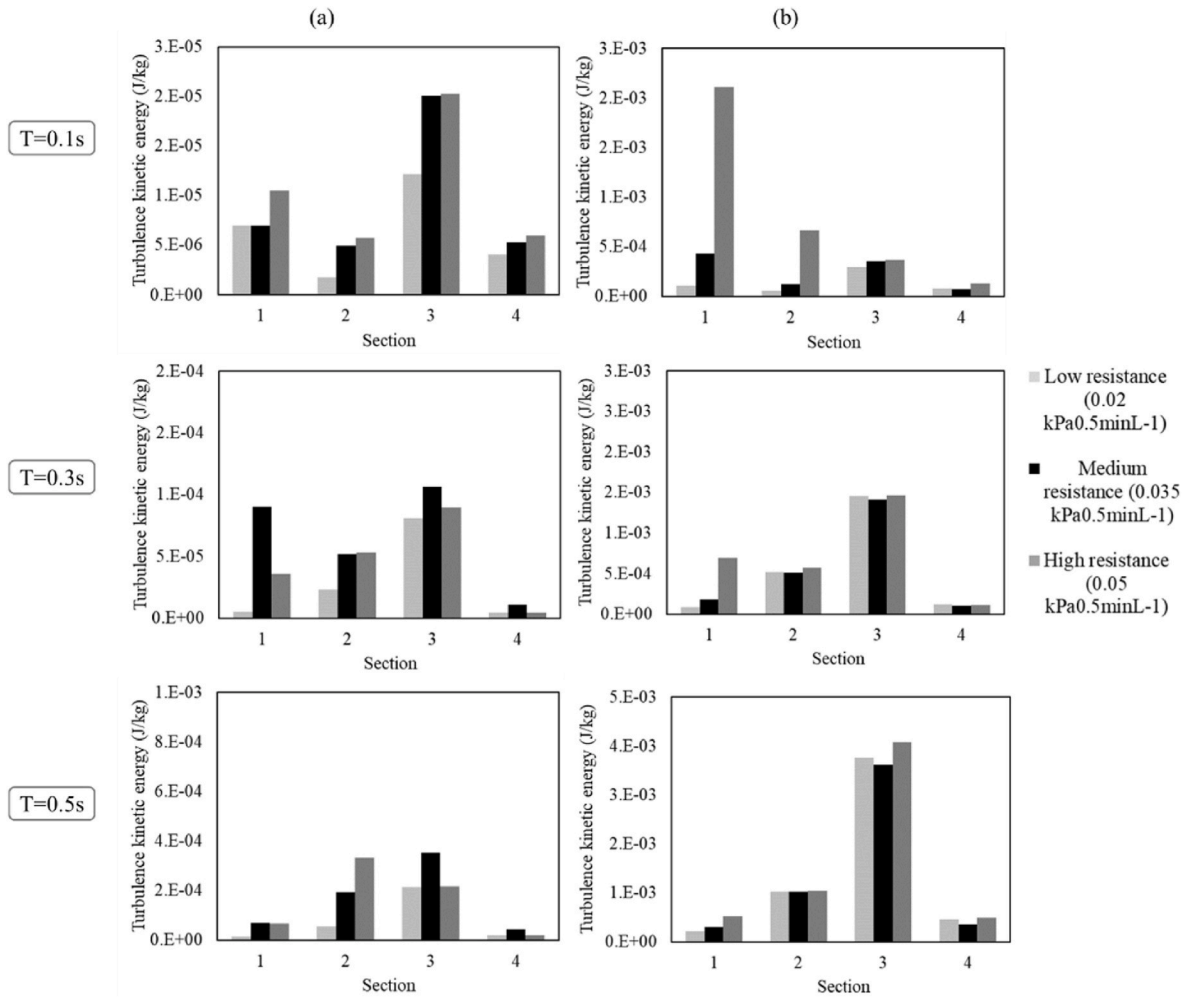

Fig. 13. Mean turbulent kinetic energy at the four sections along the realistic upper airway models. Where (a) is for 30 L/min and (b) is for 60 L/min.

Table 2
Particle deposition in the upper airway in existing studies that tested the effects of inhaler resistance. Data with an asterisk are studies that match well with the deposition result of this current work.

Reference	Geometry	Deposition for low resistance (~0.02 kPa^0.5minL^-1) (%)	Deposition for medium resistance (~0.035 kPa^0.5minL^-1) (%)	Deposition for high resistance (~0.05 kPa^0.5minL^-1) (%)	Flow condition
[9]	AIT	38* (Cylohaler)	N/A	65 (Handihaler)	Steady, 60 L/min
[9]	AIT	39* (Cylohaler)	N/A	60 (Handihaler)	Steady, 30 L/min
[12]	AIT	80 (Osmohaler)	83* (Osmohaler)	N/A	Steady, 60 L/min
[10]	AIT	N/A	67.8* (Turbuhaler)	N/A	Steady, 60 L/min
[8]	Realistic airway throat	N/A	58 (Turbuhaler)	70 (Easyhaler)	Transient, 60 L/min
[6]	Idealized pediatric throat	N/A	N/A	62 (Easyhaler)	Steady, 60 L/min
[6]	Idealized pediatric throat	N/A	N/A	70 (Easyhaler)	Steady, 30 L/min

computational models in this current study are all simulated using a transient flow profile. To understand the differences between a steady state flow and a transient flow profile and their effects on particle deposition behaviour, the volume of air associated with the profiles needs to be similar. To the best of our knowledge, no existing work has described this premise sufficiently to enable a meaningful comparison between studies. Plausible evidence to suggest that transient flow could lead to higher deposition in the upper airway can be observed in the work of Delvadia et al. [8]. This work demonstrated higher deposition in the upper airway compared to the results produced by Lindert et al. [9], despite both studies tested inhalers with very similar resistance. Delvadia et al. [8] performed their study using an Easyhaler, which has the same resistance as the Handihaler used by Lindert et al. [9].

Two other existing works that have reported deposition data that match this current work are the in-vivo studies conducted by Yang et al. [12] and Zhang et al. [13]. Both studies examined inhalers with

resistance comparable to our mid-resistance cases, and particle deposition was reported as 83 % and 70 % for Yang et al. [12] and Zhang et al. [13], respectively. These results are quite similar to this current work, where deposition is 76 %. Although this current work can only match the deposition data for using a medium inhaler resistance reported in the existing work, it demonstrates a trend of increasing upper airway deposition with higher resistance, which is a consistent observation for the data presented in Table 2. It is important to be reminded that while our results on high-resistance inhalers differ from these existing works, they are within the existing in-vivo data range obtained using SPECT imaging [12] as mentioned above.

Another observation from this study is that while increasing the flow rate increases the pharynx deposition for a given inhaler resistance (see Fig. 6), this effect is not always significant. This is consistent with the experimental work by Colthorpe et al. [7], who tested seven different inhalation profiles through a Breezhaler (~0.017 $kPa^{0.5}minL^{-1}$) to determine the dose delivery characteristics. Their results show that powder deposition in the pharynx varies only between 44 % and 47 %, despite the peak flow rate of the inhalation profiles ranging between 45 L/min to 100 L/min. These results are consistent with what we have demonstrated through our computational models. Below et al. [6] performed studies on a high-resistance inhaler (Easyhaler, ~0.048 $kPa^{0.5}minL^{-1}$) and a medium-low resistance inhaler (Novolizer, ~0.027 $kPa^{0.5}minL^{-1}$). While the Easyhaler was tested with steady-state flow rates of 28 L/min, 41 L/min and 60 L/min, the Novolizer was tested with 45 L/min, 60 L/min, 75 L/min. Despite the dissimilarity in flow rates, their results showed that the extrathoracic deposition across all the tests is fairly similar, within 10 % of discrepancies in particle deposition efficiencies between the models. Lindert et al. [9] investigated the performance of dry powder inhalers using the AIT, and showed that deposition efficiency associated with the Cyclohaler tested at 30 L/min and 60 L/min is 39 % and 38 %, respectively. They [9] performed similar work on the Handihaler based on the same flow conditions and found 65 % and 60 % deposition fractions, respectively. These results are again consistent with this current work regarding the non-significant differences in particle deposition in the human airway for a given inhaler resistance despite the large difference in peak flow rate conditions.

There are several inherent limitations that need to be considered when analysing the results of this study. First, the inhaler resistance simulated in this current work is created using a porous media. As previously mentioned, this differs from how actual inhalers currently being commercialised are designed. Modelling the inhaler may have contributed to the recirculation zones observed at the exit of the inhaler, which could have led to high particle deposition in the oral cavity, especially for the high-resistance cases. This observation is coherent with an existing study [25], where recirculation zones in the oral cavity are apparent when flow exits the inhaler into the larger cavity space. It is important to remember that having such high deposition in the mouth when using a high-resistance inhaler is possible, as has been observed through the existing in-vivo SPECT CT studies [12], albeit these studies being limited in the literature. Another limitation of the study design is that only inhalers with a small mouthpiece size were studied. Cai et al. [25] demonstrated that mouthpiece size changes humans' oropharyngeal geometry, which could subsequently produce different particle deposition profiles along the human pharynx. It would be useful to demonstrate how outcomes reported in this study may be affected using upper airway models obtained from subjects biting on inhalers with larger mouthpieces. In addition, how particle transport behaviour presented in this current study may be altered in different human airway geometries also merits further investigation. For example, there are known variations in airway geometries between genders. Previous studies [31–33] suggested that while males exhibit a higher average cross-sectional pharynx area compared to females, the cross-sectional area of the velopharynx in males is approximately 10 % smaller than that in females. Hence, fundamental differences between genders in airway properties are likely associated with their airway resistance. While the effects of pharynx resistance have not been investigated in this current work, results from the USP throat suggest that the impact of inhaler resistance is likely to diminish with the decrease of airway resistance.

Finally, while we can match our findings with existing work, it was difficult to find published studies with identical experimental conditions, such as flow rates, particle sizes and inhaler resistance. A detailed understanding of how the above factors influence the outcomes reported in this work is warranted.

5. Conclusion

Under the conditions when flow rate and mouthpiece sizes are controlled, particle deposition in the human pharynx will likely increase with higher inhaler resistance. Although the trend of increasing particle deposition with higher inhaler resistance can be observed in both the USP and geometrically realistic upper airway cases, the USP throat, being a simplified version of the human pharynx, may be limited in elucidating the true effects that inhaler resistance may produce in terms of particle deposition in the human airway. In the context of investigating inhaler resistance and its role in inhaled drug delivery, results from this work contend that the complexity of the human upper airway matters. There is also likely a threshold in resistance, beyond which it will dramatically change the flow dynamics in the human pharynx. This threshold may vary between humans depending on the complexity of their upper airway geometry.

Declaration of competing interest

All authors report no potential competing interests. The content of the manuscript has not been published or submitted for publication elsewhere, and all authors have approved the manuscript for the submission to Computers in Biology and Medicine.

Acknowledgments

This work was funded, in part, by the Australian Research Council under grants DP220100764 and DE210101549.

References

[1] S. Xiroudaki, A. Schoubben, S. Giovagnoli, D.M. Rekkas, Dry powder inhalers in the digitalization era: current status and future perspectives, Pharmaceutics 13 (9) (2021) 1455. https://www.mdpi.com/1999-4923/13/9/1455.
[2] J.L. López-Campos, W. Tan, J.B. Soriano, Global burden of COPD, Respirology 21 (1) (2016) 14–23, https://doi.org/10.1111/resp.12660.
[3] C. Nunes, A.M. Pereira, M. Morais-Almeida, Asthma costs and social impact, Asthma Res. Pract. 3 (1) (2017) 1, https://doi.org/10.1186/s40733-016-0029-3.
[4] T. Mekonnen, X. Cai, C. Burchell, H. Gholizadeh, S. Cheng, A review of upper airway physiology relevant to the delivery and deposition of inhalation aerosols, Adv. Drug Deliv. Rev. 191 (2022), 114530, https://doi.org/10.1016/j.addr.2022.114530.
[5] P.R. Byron, Drug delivery devices: issues in drug development, Proc. Am. Thorac. Soc. 1 (4) (2004) 321–328.
[6] A. Below, D. Bickmann, J. Breitkreutz, Assessing the performance of two dry powder inhalers in preschool children using an idealized pediatric upper airway model, Int. J. Pharm. 444 (1) (2013) 169–174, https://doi.org/10.1016/j.ijpharm.2013.01.007.
[7] P. Colthorpe, T. Voshaar, T. Kieckbusch, E. Cuoghi, J. Jauernig, Delivery characteristics of a low-resistance dry-powder inhaler used to deliver the long-acting muscarinic antagonist glycopyrronium, J. Drug Assess. 2 (1) (2013) 11–16, https://doi.org/10.3109/21556660.2013.766197.
[8] R. Delvadia, M. Hindle, P.W. Longest, P.R. Byron, In vitro tests for aerosol deposition II: IVIVCs for different dry powder inhalers in normal adults, J. Aerosol Med. Pulm. Drug Deliv. 26 (3) (2012) 138–144, https://doi.org/10.1089/jamp.2012.0975.
[9] S. Lindert, A. Below, J. Breitkreutz, Performance of dry powder inhalers with single dosed capsules in preschool children and adults using improved upper airway models, Pharmaceutics 6 (1) (2014) 36–51. https://www.mdpi.com/1999-4923/6/1/36.

[10] S.P. Newman, H.-K. Chan, In vitro-in vivo correlations (IVIVCs) of deposition for drugs given by oral inhalation, Adv. Drug Deliv. Rev. 167 (2020) 135–147, https://doi.org/10.1016/j.addr.2020.06.023.
[11] T. Srichana, G.P. Martin, C. Marriott, Dry powder inhalers: the influence of device resistance and powder formulation on drug and lactose deposition in vitro, Eur. J. Pharmaceut. Sci. 7 (1) (1998) 73–80, https://doi.org/10.1016/S0928-0987(98)00008-6.
[12] M.Y. Yang, J. Verschuer, Y. Shi, Y. Song, A. Katsifis, S. Eberl, K. Wong, J. D. Brannan, W. Cai, W.H. Finlay, H.-K. Chan, The effect of device resistance and inhalation flow rate on the lung deposition of orally inhaled mannitol dry powder, Int. J. Pharm. 513 (1) (2016) 294–301, https://doi.org/10.1016/j.ijpharm.2016.09.047.
[13] Y. Zhang, K. Gilbertson, W.H. Finlay, In vivo–in vitro comparison of deposition in three mouth–throat models with Qvar® and Turbuhaler® inhalers, J. Aerosol Med. 20 (3) (2007) 227–235, https://doi.org/10.1089/jam.2007.0584.
[14] A.R. Clark, J.G. Weers, R. Dhand, The confusing world of dry powder inhalers: it is all about inspiratory pressures, not inspiratory flow rates, J. Aerosol Med. Pulm. Drug Deliv. 33 (1) (2020) 1–11.
[15] D.F. Fletcher, V. Chaugule, L. Gomes dos Reis, P.M. Young, D. Traini, J. Soria, On the use of computational fluid dynamics (CFD) modelling to design improved dry powder inhalers, Pharmaceut. Res. 38 (2) (2021) 277–288, https://doi.org/10.1007/s11095-020-02981-y.
[16] K. Berkenfeld, A. Lamprecht, J.T. McConville, Devices for dry powder drug delivery to the lung, AAPS PharmSciTech 16 (2015) 479–490.
[17] S. Ghosh, J.A. Ohar, M.B. Drummond, Peak inspiratory flow rate in chronic obstructive pulmonary disease: implications for dry powder inhalers, J. Aerosol Med. Pulm. Drug Deliv. 30 (6) (2017) 381–387.
[18] P. Haidl, S. Heindl, K. Siemon, M. Bernacka, R.M. Cloes, Inhalation device requirements for patients' inhalation maneuvers, Respir. Med. 118 (2016) 65–75.
[19] D. Hira, H. Koide, S. Nakamura, T. Okada, K. Ishizeki, M. Yamaguchi, S. Koshiyama, T. Oguma, K. Ito, S. Funayama, Assessment of inhalation flow patterns of soft mist inhaler co-prescribed with dry powder inhaler using inspiratory flow meter for multi inhalation devices, PLoS One 13 (2) (2018), e0193082.
[20] D.A. Mahler, Peak inspiratory flow rate as a criterion for dry powder inhaler use in chronic obstructive pulmonary disease, Annal. American Thoracic Soc. 14 (7) (2017) 1103–1107.
[21] C. Gallagher, S. Jalalifar, F. Salehi, A. Kourmatzis, S. Cheng, A two-fluid model for powder fluidisation in turbulent channel flows, Powder Technol. 389 (2021) 163–177.
[22] B. Ma, A. Kourmatzis, Y. Zhao, R. Yang, H.-K. Chan, F. Salehi, S. Cheng, Potential effects of lingual fats on airway flow dynamics and particle deposition, Aerosol. Sci. Technol. 54 (3) (2020) 321–331, https://doi.org/10.1080/02786826.2019.1696014.
[23] J. Tu, K. Inthavong, G. Ahmadi, Computational Fluid and Particle Dynamics in the Human Respiratory System, Springer Science & Business Media, 2012.
[24] H. Chrystyn, The DiskusTM: a review of its position among dry powder inhaler devices, Int. J. Clin. Pract. 61 (6) (2007) 1022–1036, https://doi.org/10.1111/j.1742-1241.2007.01382.x.
[25] X. Cai, B. Ma, A. Kourmatzis, F. Salehi, A. Lee, D. Farina, K. Chan, S. Cheng, Potential effects of inhaler mouthpiece size on particle deposition in the human upper airway, Aerosol. Sci. Technol. 56 (9) (2022) 802–818, https://doi.org/10.1080/02786826.2022.2086034.
[26] I. Ansys, ANSYS FLUENT User's Guide, 2010. http://www.fluid.tuwien.ac.at/322057?action=AttachFile&do=get&target=flu_ug.pdf.
[27] S. Cheng, A. Kourmatzis, T. Mekonnen, H. Gholizadeh, J. Raco, L. Chen, P. Tang, H.-K. Chan, Does upper airway deformation affect drug deposition? Int. J. Pharm. 572 (2019), 118773 https://doi.org/10.1016/j.ijpharm.2019.118773.
[28] S. Lin, T.S. Premaraj, P.T. Gamage, P. Dong, S. Premaraj, L. Gu, Upper airway flow dynamics in obstructive sleep apnea patients with various apnea-hypopnea index, Life 12 (7) (2022), https://doi.org/10.3390/life12071080.
[29] F. Huang, Y. Zhang, Z.B. Tong, X.L. Chen, R.Y. Yang, A.B. Yu, Numerical investigation of deposition mechanism in three mouth–throat models, Powder Technol. 378 (2021) 724–735, https://doi.org/10.1016/j.powtec.2018.11.095.
[30] Z. Ma, A. Kourmatzis, L. Milton-McGurk, H.-K. Chan, D. Farina, S. Cheng, Simulating the effect of individual upper airway anatomical features on drug deposition, Int. J. Pharm. 628 (2022), 122219, https://doi.org/10.1016/j.ijpharm.2022.122219.
[31] R.J. Schwab, in: Sex Differences and Sleep Apnoea, vol. 54, BMJ Publishing Group Ltd, 1999, pp. 284–285.
[32] R.J. Schwab, K.B. Gupta, W.B. Gefter, L.J. Metzger, E.A. Hoffman, A.I. Pack, Upper airway and soft tissue anatomy in normal subjects and patients with sleep-disordered breathing. Significance of the lateral pharyngeal walls, Am. J. Respir. Crit. Care Med. 152 (5) (1995) 1673–1689.
[33] Y. Shigeta, T. Ogawa, J. Venturin, M. Nguyen, G.T. Clark, R. Enciso, Gender-and age-based differences in computerized tomographic measurements of the orophaynx, Oral Surg. Oral Med. Oral Pathol. Oral Radiol. Endod. 106 (4) (2008) 563–570.